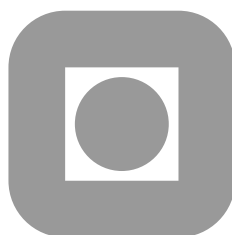NORGES TEKNISK-NATURVITENSKAPELIGE
UNIVERSITET

Some Issues Regarding the Implementation of Solvers for the Incompressible Navier–Stokes Equations

by

Bjarte Hægland and Bård Skaflestad

PREPRINT
NUMERICS NO. 1/2005

NORWEGIAN UNIVERSITY OF SCIENCE AND
TECHNOLOGY
TRONDHEIM, NORWAY

Abstract

We present the general incompressible Navier–Stokes equations. We discuss some of the challenges encountered when developing simulation code for incompressible fluid flow. Finally we compare two similar methods for solving the incompressible equations and present some results for a thermally driven cavity flow using the Boussinesq approximation to incorporate thermal source effects into the flow problem.

1   Introduction

We compare two basic methodologies for discretising the incompressible Navier–Stokes equations. The operator based integrating factor method of Maday and co-workers in [1] is a framework for generating splitting schemes for linear systems of ordinary differential equations whereas the so-called "consistent splitting schemes" recently developed by Guermond and Shen in [2] employ gradient testing of the momentum equation for evaluating the pressure at any given time step. Increased accuracy for the consistent splitting schemes is sought by rewriting the momentum equation in rotational form.

Scaling relevant physical quantities, the incompressible Navier–Stokes can be stated as

$$\frac{\partial \mathbf{u}}{\partial t} + (\mathbf{u} \cdot \nabla)\mathbf{u} + \nabla p = \tfrac{1}{Re}\Delta \mathbf{u} + \mathbf{f} \tag{1}$$

$$\operatorname{div} \mathbf{u} = 0 \tag{2}$$

in which the *Reynolds* number $Re = UL/\nu$ measures the relative influence of convection with respect to diffusion present in the physical problem. The quantities U and L are a characteristic speed and a characteristic length of the problem. Aggregate material properties of the fluid are represented by the kinematic viscosity $\nu = \mu/\rho$. Furthermore, the source term $\mathbf{f}$ incorporates any external forces such as gravity, heating, magnetic fields or other influencing phenomena.

Completing the system (1)–(2), a set of prescribed boundary conditions determines the interaction of the fluid flow with the outside world. However, the above system is inconsistent with the most general kind of boundary conditions. Adopting this model we are forced to consider only Dirichlet type velocity boundary conditions, that is the value of the velocity is prescribed on any external boundaries, and disregard any pressure forces or general surface tension effects which may be affecting the flow externally. As such equations (1)–(2) cannot be used for modelling free surface flows.

The mathematical model of incompressible fluid flows does not contain equations of state linking the pressure variable to other thermodynamic quantities such as density and temperature. The usual approach is to choose the pressure in such a way that the flow is divergence free at all times. As such, the pressure may be viewed as Lagrangian multipliers associated with the continuity equation (2).

Equations (1)–(2) are, when imposing homogeneous Dirichlet velocity boundary conditions, equivalently represented in variational form as: Find $\mathbf{u} \in V = \left(H_0^1(\Omega)\right)^d$ and $p \in \Pi = L_0^2(\Omega)$ such that

$$\frac{\partial}{\partial t}(\mathbf{u}, \mathbf{v}) + c(\mathbf{u}; \mathbf{u}, \mathbf{v}) + b(\mathbf{v}, p) = \tfrac{1}{Re}a(\mathbf{u}, \mathbf{v}) + (\mathbf{f}, \mathbf{v}), \quad \forall \mathbf{v} \in V$$

$$b(\mathbf{u}, q) = 0, \qquad \qquad \forall q \in \Pi. \tag{3}$$

in which $(\cdot, \cdot)$ denotes the regular L^2 inner product for scalar or vector valued functions. The forms occuring in (3) are explicitly given by

$$a(\mathbf{v}, \mathbf{w}) = -(\nabla \mathbf{v}, \nabla \mathbf{w}), \quad b(\mathbf{v}, q) = -(\operatorname{div} \mathbf{v}, q), \quad c(\mathbf{w}; \mathbf{z}, \mathbf{w}) = \int_\Omega [(\mathbf{w} \cdot \nabla)\,\mathbf{z}] \cdot \mathbf{v} \,\mathrm{d}\Omega.$$

Choosing finite dimensional subspaces of V and Π, respectively V_N and Π_N, based on spectral elements, the fully discretised problem becomes: Find $\mathbf{u}_N \in V_N$ and $p_N \in \Pi_N$ such that

$$\frac{\partial}{\partial t}(\mathbf{u}_N, \mathbf{v})_N + c_N(\mathbf{u}_N; \mathbf{u}_N, \mathbf{v}) + b_N(\mathbf{v}, p_N) = \frac{1}{Re} a_N(\mathbf{u}_N, \mathbf{v}) + (\mathbf{f}, \mathbf{v})_N, \quad \forall\, \mathbf{v} \in V_N \tag{4}$$
$$b_N(\mathbf{u}_N, q) = 0, \qquad\qquad\qquad \forall\, q \in \Pi_N.$$

The forms $(\cdot, \cdot)_N$, $a_N(\cdot, \cdot)$, $b_N(\cdot, \cdot)$ and $c_N(\cdot; \cdot, \cdot)$ denote the corresponding continuous forms of (3) when replacing exact integrals by numerical quadrature. As the same discrete spaces are used for both the test and trial functions, this a Galerkin approximation of the original problem (3).

Employing divergence free velocity basis functions at the outset, meaning $b(\mathbf{v}, q) = 0$ for all $\mathbf{v}$ and q thus eliminating the pressure variable from the system, existence of solutions to the continuous system (3) was proven by Leray in 1934 and Hopf in 1951. We refer the interested reader to [3] for additional detail. Furthermore, uniqueness has been established for two dimensional flows while the question of uniqueness for three dimensional flows remains an open problem. In addition, the exact conditions under which a unique pressure solution to the continuous problem exists are not known.

On the other hand, the discrete system (4) is known to have a unique velocity solution $\mathbf{u}_N$. This, however, does not hold for the pressure variable without imposing additional conditions on the pressure approximation space. One common extra requirement is imposing the discrete Ladyshenskaya–Babuška–Brezzi condition, also known as the discrete inf–sup condition. Mathematically, the discrete LBB condition reads

$$0 < \beta \equiv \inf_{q \in \Pi_N} \sup_{\mathbf{v} \in V_N} \frac{|b_N(\mathbf{v}, q)|}{\|\mathbf{v}\|_{V_N} \|q\|_{\Pi_N}} \tag{5}$$

which, ideally, should hold for constant β independent of discretisation parameters such as the polynomial degree N and number of elements in the computational domain. Realistically though, the LBB constant does depend to some extent on these parameters.

Condition (5) limits the available choices for discrete subspaces when solving the Stokes or Navier–Stokes problems. While its rôle in guaranteeing unique solutions to the linear Stokes problems is well known, the situation is a little less clear with respect to the Navier–Stokes equations. Auteri and co-workers in [4] experimentally studied the effect of using approximations which did and did not satisfy the condition in the context of pure spectral approximations. The empirical evidence gathered in this study strongly indicated that satisfying the discrete LBB condition invariably lead to qualitatively better numerical solutions. The mixed spectral element $\mathbb{P}_N$–$\mathbb{P}_{N-2}$ does satisfy the discrete LBB condition, and we have chosen to use this mixed element as the basis for defining the numerical solutions.

2 Linear solvers

Irrespective of which specific space and time discretisation scheme is chosen, solving the Navier–Stokes equations entails solving large, possibly non-symmetric, linear systems of the form

$$\begin{bmatrix} H + C & D^T \\ D & 0 \end{bmatrix} \begin{bmatrix} \mathbf{u} \\ \mathbf{p} \end{bmatrix} = \begin{bmatrix} \mathbf{F} \\ 0 \end{bmatrix} \tag{6}$$

in which H is the discrete Helmholtz operator, D is the discrete divergence operator and D^T is the discrete gradient operator. The matrix C represents the discrete convection operator, and the vector $\mathbf{F}$ is the discrete realisation of the source term present in the continuous equations.

In its complete generality, the inversion of the system matrix in (6) is prohibitively expensive. Furthermore, as the convection operator in general depends on the velocity, equation (6) is usually a *non-linear* system for which efficient solvers are hard to develop. To overcome these problems, some kind of splitting of the algebraic system is often employed. Doing the system splitting at the algebraic level rather than the continuous PDE system level makes the handling of boundary conditions easier as prescribed boundary conditions have already been incorporated into the discrete operators. However, algebraic splitting introduces other splitting errors which may or may not vanish as the resolution increases [5].

Various schemes based on splitting at the algebraic level with or without subsequent projection onto divergence free vector fields have been proposed. In [6] Quarteroni et al. list several of these schemes. In particular, the inexact factorisation

$$\begin{bmatrix} H+C & D^T \\ D & 0 \end{bmatrix} \approx \begin{bmatrix} H+C & 0 \\ D & -DH_1D^T \end{bmatrix} \begin{bmatrix} I & H_2D^T \\ 0 & I \end{bmatrix}$$

in which H_1 and H_2 are approximations of $(H+C)^{-1}$ leads to an algorithm which involves simpler system solves than the complete non-linear system.

Further algorithmic and computational simplifications are possible if the convection term is treated separately from the diffusive and pressure terms. The Lagrangian framework relying on the substantial derivative $\frac{\mathrm{D}\mathbf{u}}{\mathrm{D}t}$ led Maday and co-authors in [1] to the concept of operator integrating factor splitting methods. This framework enables explicit treatment of the convective terms which leads to algorithms generally involving resolution of discrete Helmholtz problems and a costly pressure problem involving the *consistent Poisson operator* $E = DM^{-1}D^T$ in which M denotes the mass matrix.

The Helmholtz problems in this case can be efficiently resolved using the Preconditioned Conjugate Gradient algorithm with a diagonal preconditioner $P = \mathrm{diag}(H)^{-1}$. On the other hand, the solution of linear systems of the form

$$E\mathbf{p} = \mathbf{b}$$

is strongly dependent on good preconditioners when iterative strategies are employed.

3 Operator integrating factor splitting methods – OIFS

In their 1990 paper [1], Maday and co-workers proposed a framework for generating efficient and accurate splitting schemes for the linear initial value problem

$$\frac{\mathrm{d}u}{\mathrm{d}t} = X_1(t)u + X_2(t)u + f(t), \quad u(t^0) = u^0. \tag{7}$$

The operators X_1 and X_2 in general exhibit different characteristics. In the case of the Navier–Stokes equation, X_1 may be a suitably spatially discretised convection operator, possibly involving interpolated velocity fields, whereas X_2 is a similarly discretised diffusion operator. The framework is based on integrating factors and evaluating the *action* of these operators on functions rather than explicitly forming a matrix representation of the operator itself.

Fixing $t^* > t$ and introducing the flow map $\phi_{X_1}(t, t^*)$ of the X_1 vector field from time t to time t^*, we get

$$\frac{\mathrm{d}\phi_{X_1}}{\mathrm{d}t} = -X_1(t)\,\phi_{X_1}(t, t^*), \quad \phi_{X_1}(t^*, t^*) = \mathrm{I},$$

the sign due to the flow of X_1 going *into* t^*. In the special case of $X_1(\tau_1)X_1(\tau_2) = X_1(\tau_2)X_1(\tau_1)$ for all $\tau_1, \tau_2 \in [t, t^*]$ the flow map can be explicitly represented by the matrix exponential $\exp(\int_t^{t^*} X_1(\tau)\,\mathrm{d}\tau)$. Inserting this into the initial value problem we obtain

$$\frac{\mathrm{d}}{\mathrm{d}t}\big(\phi_{X_1}(t, t^*)\, u\big) = \phi_{X_1}(t, t^*)\big(X_2(t)u + f(t)\big). \tag{8}$$

Choosing $t = t^n = t^0 + n\Delta t$, $t^* = t^{n+1}$ and discretising (8) by a BDF scheme of order k and step size Δt, we get

$$\frac{1}{\Delta t}\Big(\alpha_0 u^{n+1} + \sum_{s=1}^{k} \alpha_s \phi_{X_1}(t^{n+1-s}, t^{n+1})u^{n+1-s}\Big) = X_2(t^{n+1})u^{n+1} + f(t^{n+1}).$$

The quantities $\phi_{X_1}(t^{n+1-s}, t^{n+1})u^{n+1-s}$ for $s = 1, \ldots, k$ are end-point results of integrating the associated differential equation

$$\frac{\mathrm{d}\psi}{\mathrm{d}t} = X_1(t)\psi \tag{9}$$

from t^{n+1-s} to t^{n+1} using the initial value $\psi(t^{n+1-s}) = u^{n+1-s}$. Solving the associated system requires a separate one-step method due to different initial conditions for each quantity at each time step n. Additionally one usually wants to treat non-linear operators, such as the convection operator, explicitly to avoid expensive non-linear system solves thus requiring an explicit scheme. A common choice when the outer scheme is of high order is the well-known classic RK4 scheme of Kutta, but other alternatives are possible as well.

Discretising the Navier–Stokes equations in space by means of spectral elements yields the following system of constrained ordinary differential equations

$$M\frac{\mathrm{d}\mathbf{u}}{\mathrm{d}t} + C(\mathbf{u})\mathbf{u} + D^T\mathbf{p} = -A\mathbf{u} + M\mathbf{f}(t)$$
$$D\mathbf{u} = \mathbf{0} \tag{10}$$

with M, D^T, A, and D respectively denoting the discrete mass matrix, the discrete gradient, the discrete Laplacian, and the discrete divergence operators. Using the OIFS framework based on an outer BDF scheme of order k and treating the convection term explicitly, equation (10) is temporally discretised as

$$\begin{bmatrix} \frac{\alpha_0}{\Delta t}M + A & D^T \\ D & 0 \end{bmatrix} \begin{bmatrix} \mathbf{u}^{n+1} \\ \mathbf{p}^{n+1} \end{bmatrix} = \begin{bmatrix} M(\mathbf{f}^{n+1} - \frac{1}{\Delta t}\sum_{s=1}^{k} \alpha_s \tilde{\mathbf{u}}^{n+1-s}) \\ \mathbf{0} \end{bmatrix}. \tag{11}$$

Here $\tilde{\mathbf{u}}^{n+1-s} = \phi_{-C(\mathbf{U}(t))}(t^{n+1-s}, t^{n+1})\mathbf{u}^{n+1-s}$ in which $\mathbf{U}(t)$ is the interpolated velocity field based on $(t^{n+1-k}, \mathbf{u}^{n+1-k}), \ldots, (t^n, \mathbf{u}^n)$ and furthermore extrapolated to $(t^n, t^{n+1}]$. This particular choice of $\mathbf{U}(t)$ demands caution if using high order BDF schemes for the outer temporal discretisation.

Equation (11) is an algebraic saddle-point problem which must be resolved at each time step. A Uzawa type decoupling of the global discrete operator using the pressure variable for enforcing divergence free velocity fields is possible, but the resulting algorithm is normally too expensive in terms of computer resources. However, accepting an additional algebraic splitting error, equation (11) may be resolved at the expense of one scalar and strongly diagonally dominant Helmholtz problem for each velocity component and one system solve involving the consistent Poisson operator at each time step.

This algorithm involves the following three stages at each time step

1. Solve

$$\left(\frac{\alpha_0}{\Delta t}M + A\right)\mathbf{u}_i^* = M\left(\mathbf{f}^{n+1} - \frac{1}{\Delta t}\sum_{s=1}^{k}\alpha_s\tilde{\mathbf{u}}^{n+1-s}\right)_i - D_i^T\mathbf{p}^*$$

for each velocity component $i = 1, \ldots, d$. The pressure $\mathbf{p}^*$ is an extrapolated estimate of the pressure at the next time step. This too demands caution in the case of high-order outer stepping schemes.

2. Solve

$$(DMD^T)\,\delta\mathbf{p}^n = \frac{\alpha_0}{\Delta t}\,D\mathbf{u}^*$$

obtaining the pressure update $\delta\mathbf{p}^n = \mathbf{p}^{n+1} - \mathbf{p}^*$.

3. Update the velocity and pressure variables

$$\mathbf{p}^{n+1} = \mathbf{p}^* + \delta\mathbf{p}^n$$
$$\mathbf{u}^{n+1} = \mathbf{u}^* - \frac{\Delta t}{\alpha_0}M^{-1}D^T\delta\mathbf{p}^*,$$

the latter system being trivial as the mass matrix is diagonal.

The algebraic splitting error associated with this algorithm is explicitly represented by

$$A(\mathbf{u}^{n+1} - \mathbf{u}^*)$$

at each time step.

4 A consistent splitting scheme for the Navier–Stokes equations

Guermond and Shen in [2] develop two consistent time splitting schemes for the time dependent Navier–Stokes equations or time dependent Stokes equations. We will not derive these methods, but instead refer the reader to [2]. A method, in no need of mixed elements, given by Guermond and Shen is the consistent splitting scheme:

$$\begin{cases} \frac{1}{\Delta t}(\sum_{s=0}^{k}\alpha_s\mathbf{u}^{n+1-s}) - \frac{1}{Re}\nabla^2\mathbf{u}^{n+1} + \nabla p^{\star,n+1} = \mathbf{f}^{n+1}, & \mathbf{u}^{n+1}|_\Gamma = 0 \\ (\nabla p^{n+1}, \nabla q) = (\mathbf{f}^{n+1} - \frac{1}{Re}\nabla\times\nabla\times\mathbf{u}^{n+1}, \nabla q), & \forall q \in H^1(\Omega) \end{cases} \tag{12}$$

Here, $\{\alpha_s\}_{s=0}^{k}$ are the classical coefficients of the BDF scheme of order k, denoted BDF(k) and $p^{\star,n+1}$ is some estimation of the pressure at time $t = t^{n+1}$. As it stands, the method (12) applies to the unsteady Stokes equations. It is suggested by the authors of [2] to treat the extra convection term of the Navier–Stokes equations explicitly by including it in the right-hand side $\mathbf{f}$. As this is most likely to create an unstable scheme for high Reynolds numbers, we will instead adopt the approach used for the OIFS method in section 3 and integrate the solutions at previous time-steps forward in time to the current time. Let $X_N \subset (H_0^1(\Omega))^d$ be the discrete velocity space and $Q_N \subset H^1(\Omega)$ be the discrete pressure space. On variational form the method then reads: Given $\{\mathbf{u}^{n+1-s}\}_{s=1}^{k}$ find $\mathbf{u}^{n+1} \in X_N$ such that

$$\begin{cases} \frac{1}{\Delta t}(\alpha_0\mathbf{u}^{n+1} + \sum_{s=1}^{k}\alpha_s\tilde{\mathbf{u}}_{n+1-s}, \mathbf{v}) + \\ + \frac{1}{Re}(\nabla\mathbf{u}^{n+1}, \nabla\mathbf{v}) - (p^{\star,n+1}, \nabla\cdot\mathbf{v}) = (\mathbf{f}^{n+1}, \mathbf{v}) & \forall\mathbf{v} \in X_N \\ (\nabla p^{n+1} + \frac{1}{Re}\nabla\times\nabla\times\mathbf{u}^{n+1}, \nabla q) = (\mathbf{f}^{n+1} - (\mathbf{u}^{n+1}\cdot\nabla)\mathbf{u}^{n+1}, \nabla q) & \forall q \in Q_N. \end{cases} \tag{13}$$

where $\tilde{\mathbf{u}}_{n+1-s} = \phi_{X_1}(t_{n+1-s}, t_{n+1})u_{n+1-s}$ are the end results of integrating (9), where X_1 is the vector field associated with the convection operator, using an extrapolated convection velocity.

The scheme (13) is not well suited to finite element implementations, as the term $\nabla \times \nabla \times \mathbf{u}$ involves second order derivatives. Three terms in (13) require special discretisations. These are $\int_\Omega p \operatorname{div} \mathbf{v} \, d\Omega$, $\int_\Omega \mathbf{f} \cdot \nabla q \, d\Omega$, and $\int_\Omega \nabla \times \nabla \times \mathbf{u} \cdot \nabla q \, d\Omega$. In a single two-dimensional spectral element of size $L_x \times L_y$ when tested against the test function corresponding to node (i, j), these special discretisations become

$$\int_\Omega p \operatorname{div} \mathbf{v}_{ij} \, d\Omega = (\frac{L_y}{2}(I \otimes D^T) \, F_1 + \frac{L_x}{2}(D^T \otimes I) \, F_1)_{ij}$$

$$\int_\Omega \mathbf{f} \cdot \nabla q_{ij} \, d\Omega = (\frac{L_y}{2}(I \otimes D^T) \, F_2 + \frac{L_x}{2}(D^T \otimes I) \, F_3)_{ij}$$

$$\int_\Omega \nabla \times \nabla \times \mathbf{u} \cdot \nabla q_{ij} \, d\Omega = \quad \frac{2}{L_x}((I \otimes D^T)F_4)_{ij} - \frac{2}{L_y}((I \otimes D^T) \, F_5)_{ij}$$

$$+ \frac{2}{L_y}((D^T \otimes I)F_6)_{ij} - \frac{2}{L_x}((D^T \otimes I)F_7)_{ij},$$

where the matrices $F_k, k = 1, \dots, 7$ are given by

$(F_1)_{\alpha\beta} = \rho_\alpha \rho_\beta p_{\alpha\beta}$, $(F_2)_{\alpha\beta} = \rho_\alpha \rho_\beta g_1^{\alpha\beta}$, $(F_3)_{\alpha\beta} = \rho_\alpha \rho_\beta g_2^{\alpha\beta}$,

$(F_4)_{\alpha\beta} = \rho_\alpha \rho_\beta ((D \otimes D)U_2)_{\alpha\beta}$, $(F_5)_{\alpha\beta} = \rho_\alpha \rho_\beta ((D \otimes I)^2 U_1)_{\alpha\beta}$, $(F_6)_{\alpha\beta} = \rho_\alpha \rho_\beta ((D \otimes D)U_1)_{\alpha\beta}$,

$(F_7)_{\alpha\beta} = \rho_\alpha \rho_\beta ((I \otimes D)^2 U_2)_{\alpha\beta}$.

We note that $\{\rho_\alpha\}_\alpha$ are the quadrature weights associated to an N-th degree Gauss–Lobatto–Legendre quadrature formula on $[-1, 1]$. Furthermore, U_1 and U_2 are matricial representations of the first and second velocity components respectively.

5   Numerical results

The methods of sections 3 and 4, specialised for the simplified model problem (1)–(2), were implemented in the spectral element code described in prior technical report [7].

## 5.1   Validation of Navier–Stokes solvers

Choosing the body force term $\mathbf{f}$ in (1)–(2) to ensure an analytic solution given by

$$\mathbf{u}(x, y) = \begin{bmatrix} \pi \sin(2\pi y) \sin^2(\pi x) \sin(t) \\ -\pi \sin(2\pi x) \sin^2(\pi y) \sin(t) \end{bmatrix}, \quad p(x, y) = \cos(\pi x) \sin(\pi y) \sin(t)$$

on the unit square for $t > 0$, we study the error behaviour of the methods with respect to spatial and temporal resolution.

Figure 1 shows the L^2 global error at time $t = 1.0$ for various time step sizes using a single spectral element of polynomial degree $N = 40$. The second order BDF scheme was employed in both methods and we observe that both methods are second order with respect to time step size for this model problem.

In figure 2 the error at time $t = 0.125$ for various polynomial degrees N is displayed. The time step size $\Delta t = 2^{-12}$ was used for all simulations. Both methods appear to converge exponentially with respect to the polynomial degree of the spatial resolution.
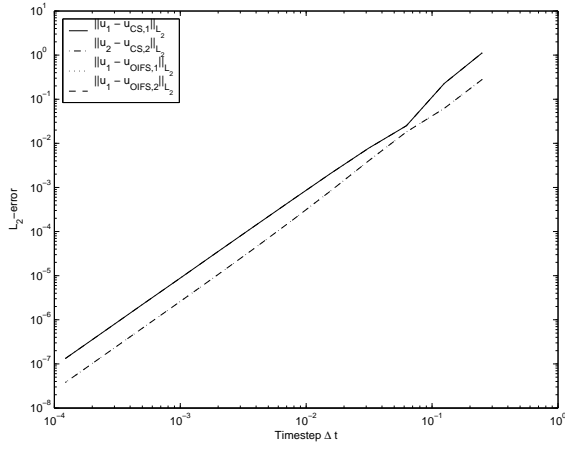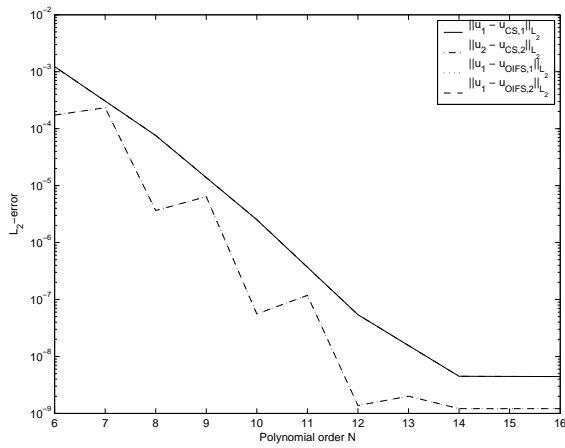
(a) Velocity convergence with respect to time step size
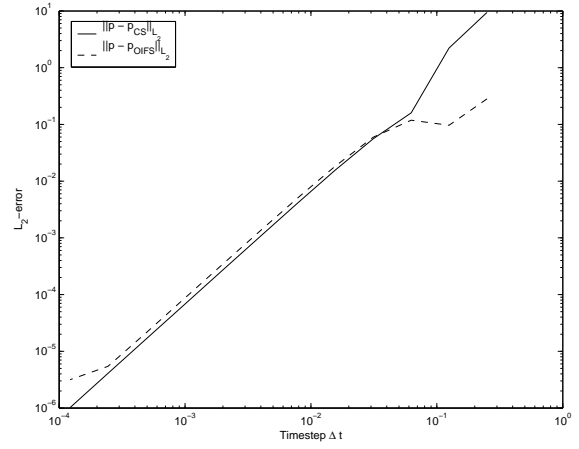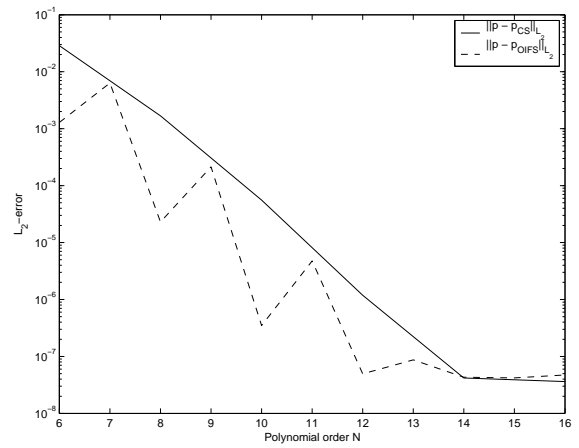
(b) Pressure convergence with respect to time step size

Figure 1: Velocity and pressure global L^2 error at $t = 1.0$

(a) Velocity convergence with respect to polynomial degree

(b) Pressure convergence with respect to polynomial degree

Figure 2: Velocity and pressure global L^2 error at $t = 0.125$

5.2 Thermally driven cavity flow

The problem considered is the two-dimensional flow of a Boussinesq fluid of Prandtl number 1.0 in a square cavity with walls of length L, see figure 3. The vertical walls are kept at constant temperatures T_h and $T_c < T_h$ for the left and right hand sides respectively. The horizontal walls are thermally insulated. Thus there is an overall heat flow across the domain in the x direction. We assume non-slip velocity boundary conditions at all walls. Assume both the velocity and
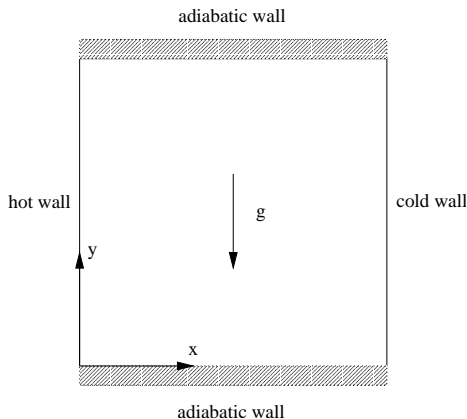

Figure 3: Domain of thermally driven cavity flow

the temperature inside the domain initial is set to zero. The hot wall heats up the nearby fluid causing it to rise due to buoyancy. This produces convection driven heat transfer and the fluid in the cavity is set in motion. We compute the steady state solution of this problem by means of a pseudo time stepping procedure.

The governing equations for the heat driven cavity flow are the incompressible Navier–Stokes equations coupled with the energy equation. Rescaling the equations, the physcial problem is modelled as the coupled system

$$\frac{\partial T}{\partial t} + (\mathbf{u} \cdot \nabla)T = \nabla^2 T$$

$$\frac{\partial \mathbf{u}}{\partial t} + (\mathbf{u} \cdot \nabla)\mathbf{u} + \nabla p = \Pr \Delta \mathbf{u} + \operatorname{Ra} \Pr T \, \mathbf{e}_2$$

$$\operatorname{div} \mathbf{u} = 0$$

with $\mathbf{e}_2$ being the unit vector in the y direction. We have employed the following scalings

$$x = \bar{x}/L, \quad y = \bar{y}/L, \qquad u = \bar{u}L/\kappa, \qquad \nu = \bar{\nu}L/\kappa,$$

$$p = \frac{\bar{p}L^2}{\rho\kappa^2}, \quad T = \frac{\bar{T} - T_c}{T_h - T_c}, \quad \operatorname{Ra} = \frac{\beta g L^3 \Delta T}{\nu\kappa}, \quad \Pr = \nu/\kappa, \quad t = \frac{\bar{t}\kappa}{L^2}$$

in which terms with bars are dimensional, while their corresponding non-dimensional quantities are unmarked. The length L of the square side is the characteristic length of the spatial domain and g is acceleration due to gravity. The fluid specific material properties ρ, ν, and κ are, respectively, the fluid's volumetric mass (density), its kinematic viscosity and thermal diffusivity. We denote by β the volumetric expansion coefficient from the Boussinesq approximation of the density alteration $\rho \approx \rho_0(1 - \beta(T - T_0))$.

Density differences in the fluid induces a buoyancy force into the system. Measuring the effect of the buoyancy forces relative to viscous forces, the Grashof number ($\operatorname{Gr} = \beta g L^3 \Delta T/\nu^2$) controls natural convection. The ratio of momentum to thermal diffusivity, known as the Prandtl number (Pr) controls the relationship between the temperature and the characteristics of the flow. The

Ra	Ref. [8]	Ref. [9]	Ref. [10]	FEM Ref. [11]	DSC Ref. [11]	Present study
10^3	3.634	3.68	3.6493	3.489	3.6434	3.6435
	(0.813)	(0.817)	(0.8125)	(0.813)	(0.8167)	(0.8050)
10^4	16.2	16.1	16.1798	16.122	15.967	15.0601
	(0.823)	(0.817)	(0.8235)	(0.815)	(0.8167)	(0.8330)
10^5	34.81	34.0	34.7741	33.39	33.51	33.3436
	(0.855)	(0.857)	(0.8535)	(0.835)	(0.85)	(0.8510)
10^6	65.33	65.4	64.6912	65.40	65.55	65.5281
	(0.851)	(0.875)	(0.8460)	(0.86)	(0.86)	(0.8505)
10^7	—	139.7	145.2666	143.56	143.06	143.8783
	—	(0.919)	(0.8845)	(0.922)	(0.92)	(0.9170)

Table 1: Value and vertical position of maximum horizontal velocity at $x = 0.5$

Rayleigh number Ra compares the destabilising buoyancy forces to the stabilising viscous and conductive mechanisms. Mathematically, $\text{Ra} = \text{Gr}\,\text{Pr}$.

The overall algorithm for solving the thermally driven cavity problem is based on time stepping until steady state. At each time step n the updated temperature T^n and updated velocity and pressure $\mathbf{u}^n$ and p^n solved alternately. All results reported for this problem are computed using the Navier–Stokes solver of section 3.

5.2.1 Comparison with earlier benchmark solutions

The problem is solved for Rayleigh numbers $\text{Ra} = 10^p$ with $p = 3, 4, 5, 6, 7$. Contour plots for the stream function, the velocity components u_1 and u_2 and the temperature field are shown in figure 4. It is seen that the solution is symmetric with respect to the centre of the cavity. At Rayleigh numbers in the range $[10^3, 10^4]$ boundary layers do not form and a stratified core is observed. For Rayleigh number 10^5 the flow changes as the we see the onset of two stratified cores, and there is a noticable temperature gradient near the vertical walls. See figure 5. As the Rayleigh number increaser further, the two cores close up at the upper left and the lower right corners. Tables 1 and 2 show maximum horizontal and vertical velocities along the lines $x = 0.5$ and $y = 0.5$ respectively. Next the maximum of both velocity components are displayed in tables 3 and 4.

An essential number is the heat flux across vertical cross sections of the domain. Figure 6 shows the Nusselt number at the hot vertical wall. As the fluid rises alongside the hot wall the fluid gradually becomes warmer and thus reducing the heat flux from the wall to the fluid as the y coordinate increases. The curves in figure 6 represent Rayleigh numbers $10^k, k = 3, \ldots, 7$ with the dotted line being $\text{Ra} = 10^3$, the solid line being $\text{Ra} = 10^4$, the dash-dotted line being $\text{Ra} = 10^5$, the dashed line being $\text{Ra} = 10^6$, and the bold solid line being $\text{Ra} = 10^7$.

In table 5 the average values of the Nusselt number at the hot wall, the line $x = 0.5$ and over the entire domain are found in table 5.

6 Concluding remarks and future work

We have presented the naturally heat driven convection in a vertical cavity. Our results compare well to those of previous studies. We experienced some difficulties computing the steady state solution for Rayleigh numbers greater than 10^6. The reason for this is not clear, but likely

Ra = 10^3

Ra = 10^4

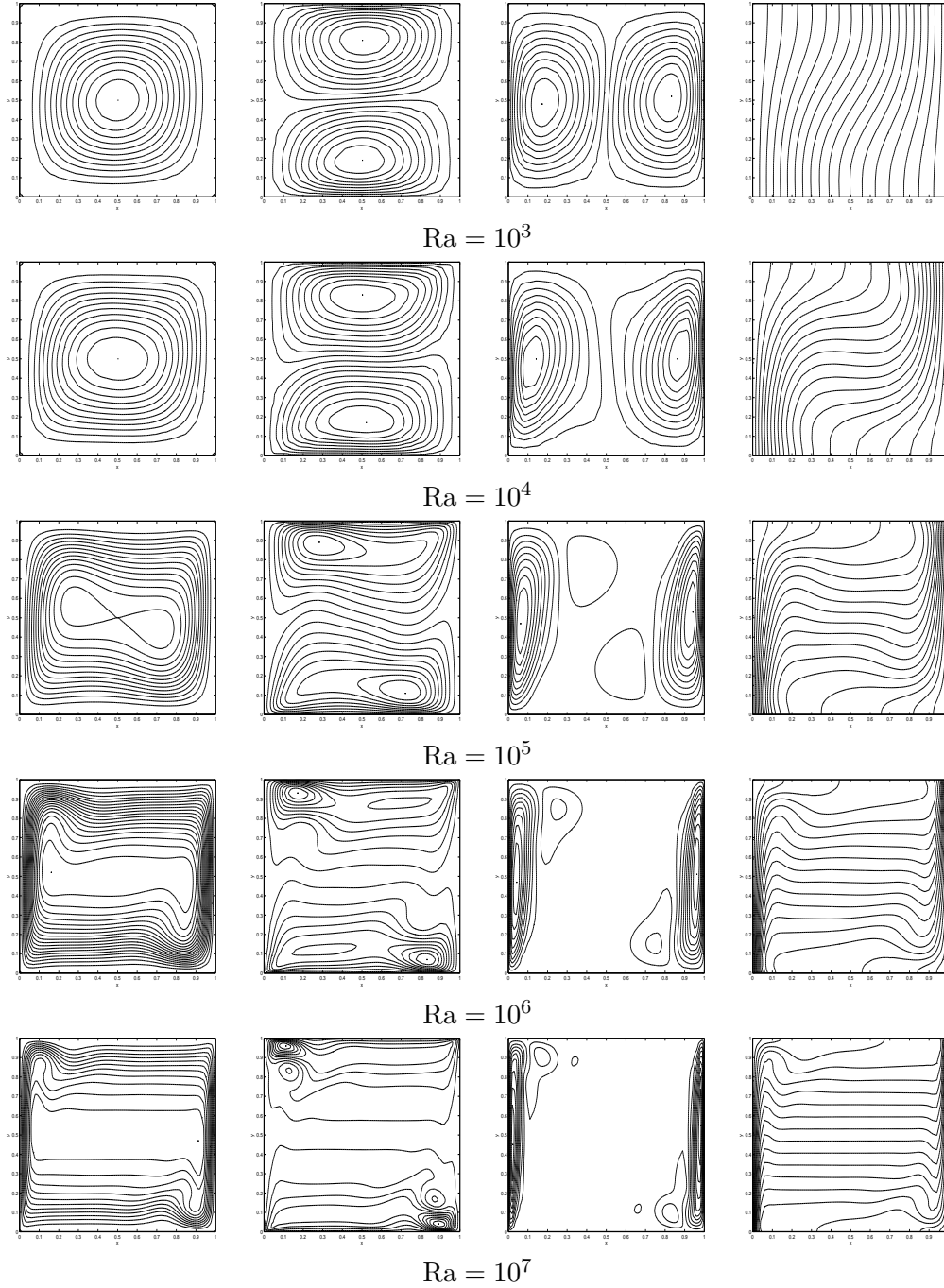Ra = 10^5

Ra = 10^6

Ra = 10^7

Figure 4: Natural convection in a cavity. From the left: stream lines, u_1 and u_2 velocities and temperature contour plots.
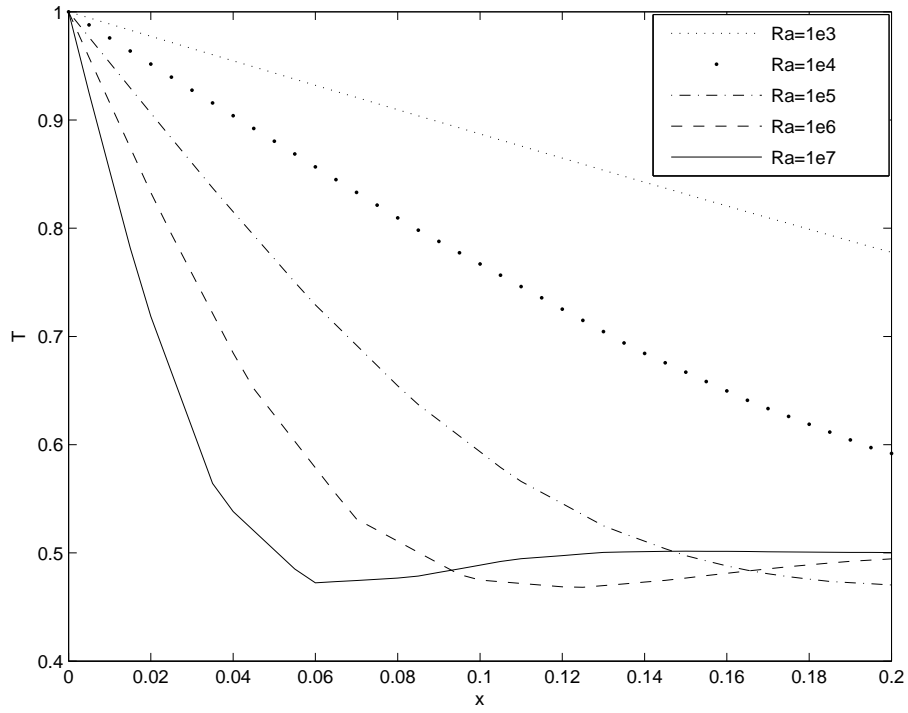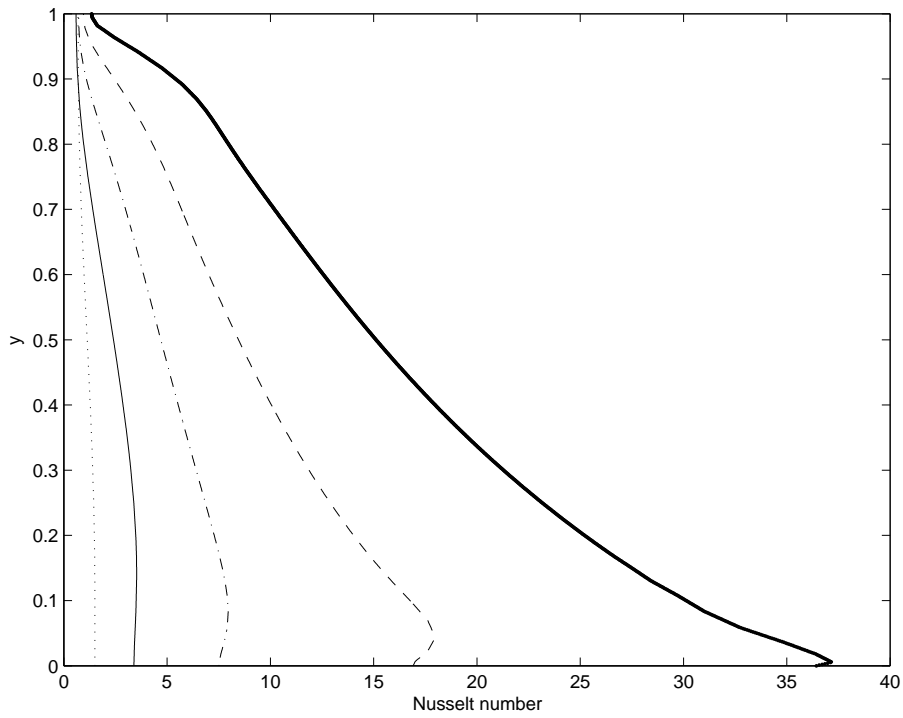
Figure 5: Temperature at $y = 0.5$.

Figure 6: Nusselt number at vertical walls

Ra	Ref. [8]	Ref. [12]	Ref. [13]	Ref. [9]	Ref. [10]	FEM Ref. [11]	DSC Ref. [11]	Present study
10^3	3.679	—	3.692	3.73	3.6962	3.686	3.686	3.6815
	(0.179)	—	—	(0.1827)	(0.1790)	(0.188)	(0.183)	(0.1670)
10^4	19.51	19.62	19.63	19.9	19.6177	19.79	19.98	19.3323
	(0.12)	—	—	(0.1246)	(0.1195)	(0.12)	(0.117)	(0.1380)
10^5	68.22	68.62	68.85	70.0	68.6920	70.63	70.81	69.6205
	(0.066)	—	—	(0.068)	(0.0665)	(0.072)	(0.070)	(0.0590)
10^6	216.75	232.97	221.6	228	220.8331	227.11	227.24	223.8965
	(0.0387)	—	—	(0.039)	(0.0380)	(0.040)	(0.040)	(0.0430)
10^7	—	717.04	702.3	698	703.2536	714.48	714.47	698.4685
	—	—	—	(0.0235)	(0.0215)	(0.022)	(0.021)	(0.0180)

Table 2: Value and horizontal position of maximum vertical velocity at $y = 0.5$

Ra	FEM Ref. [11]	DSC Ref. [11]	Present study
10^3	3.657	3.648	3.6435
	(0.512,0.812)	(0.516,0.816)	(0.5000, 0.8050)
10^4	16.14	15.968	15.9693
	(0.489,0.812)	(0.5, 0.816)	(0.4720, 0.8330)
10^5	41.88	41.82	41.4583
	(0.281, 0.881)	(0.29, 0.88)	(0.2750, 0.8920)
10^6	114.3	114.53	113.9703
	(0.164, 0.927)	(0.173, 0.93)	(0.1730, 0.9300)
10^7	339.45	339.67	333.6303
	(0.108,0.963)	(0.1067,0.96)	(0.1080, 0.9640)

Table 3: Value and position of maximum horizontal velocity over entire domain

Ra	FEM Ref. [11]	DSC Ref. [11]	Present study
10^3	3.692	3.69	3.6831
	(0.188,0.488)	(0.183,0.483)	(0.1670, 0.4720)
10^4	19.91	20.1	19.3323
	(0.119,0.465)	(0.1167, 0.467)	(0.1380, 0.5000)
10^5	70.81	70.83	69.9157
	(0.07, 0.488)	(0.07, 0.49)	(0.0590, 0.4640)
10^6	228.05	227.88	224.0141
	(0.037, 0.441)	(0.04, 0.47)	(0.0430, 0.4770)
10^7	720.54	720.43	707.4802
	(0.021,0.439)	(0.02, 0.044)	(0.0180, 0.4170)

Table 4: Value and position of maximum vertical velocity over entire domain

Ra	Nu	Ref. [8]	Ref. [13]	Ref. [9]	FEM Ref. [11]	DSC Ref. [11]	Present study
10^3	$\overline{\mathrm{Nu}}_0$	1.117	—	—	—	—	1.1186
	$\overline{\mathrm{Nu}}_{1/2}$	1.118	—	—	—	—	1.1133
	$\overline{\mathrm{Nu}}$	1.12	1.117	1.074	1.117	1.073	1.1175
10^4	$\overline{\mathrm{Nu}}_0$	2.238	—	—	—	—	2.2460
	$\overline{\mathrm{Nu}}_{1/2}$	2.243	—	—	—	—	2.1729
	$\overline{\mathrm{Nu}}$	2.243	2.243	2.084	2.254	2.155	2.2200
10^5	$\overline{\mathrm{Nu}}_0$	4.509	—	—	—	—	4.6009
	$\overline{\mathrm{Nu}}_{1/2}$	4.519	—	—	—	—	4.5768
	$\overline{\mathrm{Nu}}$	4.52	4.521	4.3	4.598	4.352	4.5894
10^6	$\overline{\mathrm{Nu}}_0$	8.817	—	—	—	—	8.9940
	$\overline{\mathrm{Nu}}_{1/2}$	8.799	—	—	—	—	8.9627
	$\overline{\mathrm{Nu}}$	8.8	8.806	8.743	8.976	8.632	8.9868
10^7	$\overline{\mathrm{Nu}}_0$	—	—	—	—	—	16.4780
	$\overline{\mathrm{Nu}}_{1/2}$	—	—	—	—	—	16.7031
	$\overline{\mathrm{Nu}}$	—	—	—	—	—	16.8034

Table 5: Average Nusselt number at hot wall $x = 0$ $(\overline{\mathrm{Nu}}_0)$, horizontal center $x = 0.5$ $(\overline{\mathrm{Nu}}_{1/2})$ and over entire domain $(\overline{\mathrm{Nu}})$ for varying Rayleigh numbers.

related to large temperature gradients at the vertical wall at high Rayleigh numbers. Although all numerical experiments for comparison were run on a mesh based on uniform elemental subdivision, a subsequent run of the $\mathrm{Ra} = 10^7$ case using a manually solution adapted mesh produced the same results as the original experiment. However, the computational cost in obtaining this solution was less than required for the uniform discretisation, thus proving that adapative methods perfom better. Hence some method for automatic mesh adaptation is desirable.

The Helmholtz operator $H = \frac{\alpha_0}{\Delta t} M + A$ is diagonally dominant, particularly for small step sizes, and the Helmholtz problem for predicting the velocity field in the Navier–Stokes solver is hence effectively preconditioned by the inverse of the diagonal of H. However, at the time of this report no preconditioning strategy is employed when resolving the pressure problem. As this is a relatively costly component in the overall algorithm, there is undoubtedly some efficiency gain in adopting some preconditioning procedure for this problem. Fischer [14] describes a finite element based preconditioning technique, and implementing this method is a prioritised task in future development.

Although the code is capable of describing different boundary conditions (constant or non-constant) for any number of unknowns, the Navier–Stokes solvers are only capable of handling homogeneous Dirichlet conditions. Some change is needed to remedy this restriction.

The code is largely agnostic with respect of the physical dimension of the actual problem being solved. However, some tuning and additional benchmarking of two-dimensional problems is likely needed before three-dimensional problems are successfully handled. Moreover, effective turbulence modelling for both two and three dimensional cases is needed in order to handle eg. convection dominated flows around immersed bodies.

Many important problems include a free surface or a fluid/structure interface, and hence introduce a time-dependent fluid domain. Such problems need a solver for the mesh motion and arbitrary Lagrangian–Eulerian (ALE) formulation of the fluid solver.

The Fortran 95 programming language is very expressive in the numerical method problem domain, giving code which is highly maintainable if written according to sound practices. As such,

the language is an excellent tool for implementing code solving a variety of simulation problems. However, data input and output is not as flexible as in other programming languages, and, in addition, Fortran's features for advanced data structures is still somewhat limited with respect to languages designed to directly support the object oriented paradigm. Consequently, a mixed language implementation exploiting Fortran's excellent performance for the computationally intensive parts while expressing I/O and high level abstracting data structures in another language may be beneficial.

Furthermore, the performance of the code may be greatly improved by a parallel implementation. All data structures are represented in a local, element-by-element fashion. The discrete operators may then be naturally represented as a series of independent, parallell components coupled by efficient interprocessor communication, such as the facilities offered by the MPI standard. The authors will investigate parallel implementation in the future.

References

[1] Y. Maday, A. Patera, and E.M. Rønquist. An operator-integration-factor-splitting method for time-dependent problems: Application to incompressible fluid flow. *J. Sci. Comp.*, 5:263–292, 1990.

[2] J.L. Guermond and Jie Shen. A new class of truly consistent splitting schemes for incompressible flows. *Journal of Computational Physics*, 192:262–276, 2003.

[3] A. Quarteroni and A. Valli. *Numerical Approximation of Partial Differential Equations*, volume 2. Springer, 1997.

[4] F. Auteri, J.-L. Guermond, and N. Parolini. Role of the LBB Condition in Weak Spectral Projection Methods. *Journal of Computational Physics*, 174:405–420, 2001.

[5] M.O. Deville, P.F. Fischer, and E.H. Mund. *High-Order Methods for Incompressible Fluid Flow*, volume 9 of *Cambridge Monographs on Applied and Computational Mathematics*. Cambridge University Press, 2003.

[6] A. Quarteroni, F. Saleri, and A. Veneziani. Factorization methods for the numerical approximation of Navier–Stokes equations. *Comput. Methods Appl. Mech. Engrg*, 188:505–526, 2000.

[7] B. Hægland and B. Skaflestad. Design and Implementation of a Spectral Element Code. Technical Report 3, Dept. Math. Sciences, Norwegian University of Science and Technology, 2004. Available in electronic form at `http://www.math.ntnu.no/preprint/numerics/2004/N3-2004.pdf`.

[8] G. De Vahl Davis. Naural Convection of Air in a Square Cavity: A Bench Mark Solution. *International Journal for Numerical Methods in Fluids*, 3:249–264, 1983.

[9] M.T. Manzari. An explicit finite element algorithm for convection heat transfer problems. *International Journal of Numerical Methods for Heat & Fluid Flow*, 9(8):860–877, 1999.

[10] D.A. Mayne, A.S. Usmani, and M. Crapper. *h*-adaptive finite element solution of high Rayleigh number thermally driven cavity problem. *International Journal of Numerical Methods for Heat & Fluid Flow*, 10(6):598–615, 1999.

[11] D.C. Wan, B.V. Patnaik, and G.W. Wei. A New Benchmark Quality Solution for the Buoyancy-Driven Cavity by Discrete Singular Convolution. *Numerical Heat Transfer, Taylor & Francis*, 2001.

[12] B. Ramaswamy, T.C. Jue, and J.E. Akin. Semi-Implicit and Explicit Finite Element Schemes for Coupled Fluid/Thermal Problems. *International Journal for Numerical Methods in Engineering*, 34:675–696, 1992.

[13] N. Massarotti, P. Nithiarasu, and O.C. Zienkiewicz. Characteristic-based-split (CBS) algorithm for incompressible flow problems with heat transfer. *International Journal of Numerical Methods for Heat & Fluid Flow*, 8(8):969–990, 1998.

[14] P.F. Fischer. An overlapping Schwarz method for spectral element solution of the incompressible Navier–Stokes equations. *Journal of Computational Physics*, 133:84–101, 1997.

[15] C. Canuto, Y. Hussaini, A. Quarteroni, and T.A. Zang. *Spectral Methods in Fluid Dynamics*. Springer Series in Computational Physics. Springer Verlag, Berlin, 1988.

[16] W.J. Gordon and C.A. Hall. Construction of Curvilinear Co-ordinate Systems and Application to Mesh Generation. *International Journal for Numerical Methods in Engineering*, 7:461–477, 1973.

[17] H.P. Langtangen and A. Tveito, editors. *Advanced Topics in Computational Partial Differential Equations*, volume 33 of *Lecture Notes in Computational Science and Engineering*. Springer Verlag, 2003.

[18] E.M. Rønquist. *Optimal Spectral Element Methods for the Unsteady Three-Dimensional Incompressible Navier–Stokes Equations*. PhD thesis, Massachusets Institute of Technology, Cambridge, MA, 1988.

[19] E.M. Rønquist. A Domain Decomposition Solver for the Steady Navier–Stokes Equations. In A. Ilin and R. Scott, editors, *Proceedings of the Third International Conference on Spectral and High-Order Methods*. Huston J. of Mathematics, 1996.

[20] E.M. Rønquist. The Design of a Finite Element/Spectral Element Code for Incompressible Fluid Flow. In M.E. Henderson, C.R. Anderson, and S.L. Lyons, editors, *Proceedings of the 1998 Workshop on Object Oriented Methods for Interoperable Scientific and Engineering Computing*, IBM TJ Watson Research Center, 1999. SIAM.

[21] B. Smith, P. Bjørstad, and W. Gropp. *Domain Decomposition: Parallel Multilevel Methods for Elliptic Partial Differential Equations*. Cambridge University Press, 1996.

[22] R.N. Yurkovich, D.D. Liu, and P.C. Chen. The state-of-the-art of unsteady aerodynamics for high performance aircraft. Number AIAA Paper No. 2001-0428 in 39th AIAA Aerospace Science Meeting & Exhibit, Reno, Nevada, January 8–11 2001. AIAA.

[23] J.D. Lambert. *Numerical Methods for Ordinary Differential System*. Wiley, 1991.

[24] S.C. Brenner and L.R. Scott. *The Mathematical Theory of Finite Element Methods*, volume 15 of *Texts in Applied Mathematics*. Springer-Verlag New York, second edition, 2002.

[25] S. Paolucci and D.R. Chenoweth. Transistion to Chaos in a Differentially Heated Vertical Cavity. *J. Fluid Mech.*, 201:379–410, 1989.

[26] A.J. Chorin. The numerical solution of the Navier–Stokes equations for an incompressible fluid. *Amer. Math. Soc.*, 73:928–931, 1967.

[27] A.J. Chorin. Numerical solution of the Navier–Stokes equations. *Math. Comput.*, 22:745–762, 1968.

[28] R. Temam. Sur l'approximation de la solution des equations de Navier–Stokes par la metode de pas fractionnaires. *Arch. Rat. Mech. Anal.*, 33:377–385, 1969.

[29] R. Temam. Navier–Stokes Equations: Theory and Numerical Analysis. *AMS Chelsea Publishing*, 2001.

[30] L. Quartapelle. *Numerical Solution of the incompressible Navier–Stokes Equations*. Number 113 in International Series of Numerical Mathematics. Birkh auser Verlag, 1993.